HHS Public Access

Author manuscript

*Neurobiol Dis*. Author manuscript; available in PMC 2020 April 14.

Published in final edited form as:

*Neurobiol Dis*. 2020 March ; 136: 104713. doi:10.1016/j.nbd.2019.104713.

# Sustained neuronal and microglial alterations are associated with diverse neurobehavioral dysfunction long after experimental brain injury

**Rodney M. Ritzel**[a,1], **Yun Li**[a,1], **Junyun He**[a], **Niaz Khan**[a], **Sarah J. Doran**[a], **Alan I. Faden**[a,b], **Junfang Wu**[a,b,*]

[a]Department of Anesthesiology and Center for Shock, Trauma and Anesthesiology Research (STAR), University of Maryland, School of Medicine, Baltimore, MD 21201, USA

[b]University of Maryland, Center to Advance Chronic Pain. Research, University of Maryland, Baltimore, MD 21201, USA

## Abstract

Traumatic brain injury (TBI) can cause progressive neurodegeneration, sustained neuroinflammation and chronic neurological dysfunction. Few experimental studies have explored the long-term neurobehavioral and functional cellular changes beyond several months. The present study examined the effects of a single moderate-level TBI on functional outcome 8 months after injury. Male C57BL/6 mice were subjected to controlled cortical impact injury and followed for changes in motor performance, learning and memory, as well as depressive-like and social behavior. We also used a novel flow cytometry approach to assess cellular functions in freshly isolated neurons and microglia from the injured tissue. There were marked and diverse, sustained neurobehavioral changes in injured mice. Compared to sham controls, chronic TBI mice showed long-term deficits in gait dynamics, nest building, spatial working memory and recognition memory. The tail suspension, forced swim, and sucrose consumption tests showed a marked depressive-like phenotype that was associated with impaired sociability. At the cellular level, there were lower numbers of $Thy1^{+}Tuj1^{+}$ neurons and higher numbers of activated $CD45^{lo}CD11b^{+}$ microglia. Functionally, both neurons and microglia exhibited significantly higher levels of oxidative stress after injury. Microglia exhibited chronic deficits in phagocytosis of *E. coli* bacteria, and increased uptake of myelin and dying neurons. Living neurons showed decreased expression of synaptophysin and postsynaptic density (PSD)-95, along with greater numbers of microtubule-associated protein light chain 3 (LC3)-positive autophagosomes and increased mitochondrial mass that suggest dysregulation of autophagy. In summary, the late neurobehavioral changes found after murine TBI are similar to those found chronically after moderate-severe human head injury. Importantly, such changes are associated with microglial dysfunction and changes in neuronal activity.



*Corresponding author at: 685 W Baltimore St., Baltimore, MD 21201, USA, junfang.wu@som.umaryland.edu (J. Wu).

[1]Both authors contributed equally

Declaration of Competing of Interest

The authors declare that they have no competing financial interests.

**Keywords**

Chronic traumatic brain injury; Neurodegeneration; Neuroinflammation; Cognition; Depression; Microglia

## 1. Introduction

Traumatic brain injury (TBI) is the leading cause of death in the first forty years of life, and accounts for 30% of all injury-related deaths (Popescu et al., 2015; Taylor et al., 2017). An estimated 1.1% of the US population experience lifelong disabilities as a consequence of TBI, limiting their ability to work and perform daily activities (Zaloshnja et al., 2008). Patients who survive head injuries often present with disabilities that persist for decades, including sensorimotor impairment, learning and memory deficits, and emotional dysregulation. All of these are associated with posttraumatic delayed secondary injury cascades including chronic neuroinflammation and neurodegeneration (Hay et al., 2016; Loane et al., 2014; Masel and DeWitt, 2010). Recent clinical longitudinal data and experimental studies have significantly revised the outdated concept that TBI is an acute neurological disorder. Instead, persistent and diffuse neuroinflammation in the injured brain, with progressive neurodegeneration, can continue for months to years (Crane et al., 2016; Cruz-Haces et al., 2017; DeKosky and Asken, 2017; Johnson et al., 2017; Raj et al., 2017).

Currently, insights into the mechanisms that transform the initial biomechanical injury into a chronic neuroinflammation and neurodegenerative process remain unclear. Although studies have described the chronic neuropathological changes and associated neurological dysfunction after experimental TBI, most observations have been limited to only a few months and focus primarily on histological analyses of fixed tissue samples (Campos-Pires et al., 2019; Cheng et al., 2019; Davies et al., 2018; Loane et al., 2014; Mouzon et al., 2014; Mouzon et al., 2018; Nakagawa et al., 1999; Shear et al., 2004). In particularly, functional assessment at the cellular levels such as neurons and microglia is largely lacking following chronic TBI. Limited evidence regarding outcome assessments several months (or decades in human years) after experimental TBI indicate that sensorimotor and cognitive deficits persist up to one year, with controlled cortical impact (CCI) and fluid percussion injury (FPI) models both resulting in progressive tissue loss and glial activation (Osier et al., 2015; Wojnarowicz et al., 2017). The immunological changes coincident with long-term neurological decline, however, remain open for investigation. More specifically, data to support the notion that TBI chronically alters neuro-immune home-ostasis by inducing lasting, aberrant changes in neuronal and microglial function is sparse. In an effort to better understand the complex role of aging on the behavioral sequelae and cellular pathophysiology to TBI, we followed young male sham and injured mice for eight months after CCI and evaluated them using a battery of behavioral tests and flow cytometry. We demonstrate significant diverse neurological deficits, including marked depressive-like behavior and impaired social behavior, which are associated with neuronal and microglial dysfunction at eight months after injury.

## 2. Materials and methods

### 2.1. Animals and controlled cortical impact injury

Adult male C57BL/6 mice at 10–12 weeks old (22–25 g) were obtained from Taconic. After being anesthetized with isoflurane, the subject mice received controlled cortical impact (CCI) using a custom microprocessor-controlled and compressed air driven pneumatic impactor as described (Piao et al., 2013; Zhao et al., 2012). Briefly, a 10-mm midline incision was made over the skull, the skin and fascia were retracted, and a 4-mm craniotomy was made on the central aspect of the left parietal bone of mice under surgical anesthesia. A moderate injury was induced by a 3.5-mm diameter tip with impact velocity of 6 m/s and a deformation depth of 2 mm. In sham mice, same procedure was performed except for the impact. The number of mice in each study is indicated in the figure legends. All surgical procedures and animal experiments were performed under protocols approved by the University of Maryland School of Medicine Institutional Animal Care and Use Committee (IACUC). The surgical procedures were performed by the same investigator and all behavioral tests were carried our using the same equipment by blinded experimenters. SLICK-A transgenic mice were purchased from a commercial vendor (Jackson Laboratories, B6.Cg-Tg(Thy1-cre/ERT2,-EYFP)AGfng/J; stock no. 007606) and used for the sole purpose of confirming our neuronal gating strategy for identification by flow cytometry (Young et al., 2008).

### 2.2. CatWalk XT automated gait analysis

Motor coordination was performed and analyzed using the CatWalkXT automated system (Noldus; RRID:SCR_004074) (Matyas et al., 2017). Each mouse underwent only one testing session at 26 weeks after TBI to maintain situational novelty and encourage exploration of the CatWalk. Data acquisition took place in a darkened room with the same researcher handling each subject. The CatWalk itself features a red overhead lamp and green illuminated walkway, which responds to the pressure of the animals' weights and obtains live foot print videos. Each mouse was first placed in the open end of the CatWalk under the red ceiling light and allowed to walk across the walkway to the darkened escape enclosure. A minimum of three valid runs, or complete walkway crossings, were obtained for each subject. Trials in which the animal stopped partway across or turned around during a run were excluded from analysis.

### 2.3. Assessment of general well-being by nest building test

Nesting behavior is an ethologically relevant indicator of welfare. For nest building test, we followed the method described by Deacon et al. in Nature Protocols (Deacon, 2006). At 1 h before the dark phase begins in the animal facility, all mice to be tested were transferred to individual cages with wood-chip bedding but no environmental enrichment items. After measuring and recording the weight of the cotton nestlets used, place one piece (approximately 2–3 g) into each cage. The next morning, weigh any untorn nestlet pieces after brushing off the loose material and bedding. A rating scale of 1–5 is used to assess the nests and assign scores to each nest built by the tested nest. Briefly, a score of 1 would mean the nestlet has not been noticeably touched with > 90% of the cotton nestlet intact; a score of 2 would indicate a nestlet partially torn with 50–90% remaining intact; a score of 3

would mean a nestlet mostly shredded but often no identifiable nest site; a score of 4 is an identifiable but flat nest with > 90% of the nestlet torn and gathered but the nest is flat with < 50% of its walls higher than mouse body height; while a score of 5 points to a near perfect nest with > 90% of the nestlet torn and forming a crater.

### 2.4. Depressive-like behavioral tests

The tail-suspension (TS) test is based on the observation that mice develop an immobile posture when placed in an inescapable hemodynamic stress of being hung by their tail. The TS was performed on 27 weeks as described previously (Wu et al., 2016; Zhao et al., 2012), with small modifications. Each mouse was suspended at a height of 50 cm using adhesive tape placed approximately 1 cm from the tip of its tail. The duration of immobility was recorded throughout the 5-min test period. The definition of immobility was passive hanging and complete motionlessness.

The mouse forced swim test (FST) is based on the assumption that when placing an animal in a container filled with water, it will first make efforts to escape but eventually will exhibit immobility that may be considered to reflect a measure of behavioral despair. The FST was performed on 27 weeks as previously described (Wu et al., 2016). Briefly, mice were placed in a transparent plastic cylinder (25 cm high × 20 cm diameter) filled with water (22–23 °C; 22 cm in depth). The duration of immobility was recorded throughout the 6 min test period. Immobility was characterized as a lack of any movement.

The sucrose preference (SP) test was used to evaluate interest in seeking a sweet rewarding drink relative to plain water on 27 weeks as described previously (Wu et al., 2016; Wu et al., 2014). A diminished preference for the sweetened drink is a sign of anhedonia, indicating depression-like behavior. Briefly, two inserts were placed in each cage—one with plain water in the normal (back) position and the sweetened water (0.3% saccharine) positioned at the front. After 24 h, the positions of sweetened and tap water were switched to avoid placement preference. At 48 h after initiation of the test, the water pouches, food, and mice were weighed and recorded. The sucrose preference was calculated by dividing consumption of sweetened water by total consumption of water (sweetened water plus plain water). The food preference also was calculated as a control to demonstrate that mice did not show a place preference.

### 2.5. Social interaction test

Social interaction was assessed with the sociability and preference test originally designed by Crawley et al. (Moy et al., 2004), using a three-chambered rectangular apparatus made of Plexiglas with each chamber equally divided at 20 (width) × 40 (length) × 23 (height) cm. An open middle section allows free access to each chamber and two identical, wire cup-like containers that are large enough to hold a single mouse. The experiment consists of three 10 min phases with the test mouse starting off in the middle chamber for each phase. In the first phase, the test mouse is allowed to freely explore all three chambers for a time period of 10 min and habituate to the novel environment. The second phase consists of a stimulus mouse and an object of interest randomly assigned to either the left or right chamber, which the mouse the again allowed to explore for a duration of 10 min. In the third phase, the object

is exchanged for a second, unfamiliar mouse. The contact time of the test mouse with each empty cup in the first phase, with the mouse and object in the second phase and with each mouse in the third phase are recorded as a test readout.

### 2.6. Assessment of cognitive function

Y-maze spontaneous alternation test assesses spatial working memory (Piao et al., 2013; Wu et al., 2016). The percentage of alternation is calculated on 26 weeks post-injury using the following equation: total alternations x 100/(total arm entries - 2). If a mouse scored significantly above 50% alternations (the chance level for choosing the unfamiliar arm), this was indicative of functional working memory.

Novel object recognition (NOR) evaluated non-spatial hippocampal- mediated memory on 26 weeks post-injury as previously reported (Piao et al., 2013; Wu et al., 2016). Briefly, 24 h after training with two identical objects (sample phase), object recognition was tested by substituting a novel object for a familiar training object (choice phase). The objects were used in a counterbalanced way to minimize any induced object preference. Each object was used equally as a familiar object and as a novel object. Novel object location was counterbalanced across mice (left or right side of the chamber). Time spent with two identical objects was recorded; because mice inherently prefer to explore novel objects, a preference for the novel object (more time than chance [10s] spent with the novel object) indicates intact memory for the familiar object.

### 2.7. Flow cytometry and ex vivo cellular function assays

Mice were perfused with 40 mL of cold PBS and the ipsilateral (i.e., craniotomy-side) hemisphere was isolated. The olfactory bulb and cerebellum were removed and the remaining hemispheres were placed separately in complete Roswell Park Memorial Institute (RPMI) 1640 (Lonza) medium and mechanically and enzymatically digested in collagenase/dispase (1 mg/mL; Roche), papain (5 U/mL; Worthington Biochemical), EDTA (1:50; Invitrogen), and DNAse (10 mg/mL; Roche Diagnostics) for 1 h at 37 °C on a shaking incubator (200 rpm). The cell suspension was washed twice with RPMI, filtered through a 70-μm filter, and RPMI was added to a final volume of 5 mL/hemisphere and kept on ice. 500 μl of cells were then transferred into FACS tubes and washed with FACS buffer. Cells were then blocked with anti-mouse CD16/CD32 Fc Block (clone 93, Biolegend) prior to staining with primary antibody-conjugated flourophores: CD45-eF450 (clone 30-F11), CD11b-APCeF780 (clone M1/70), Ly6C-APC or –AF700 (clone HK1.4), and Thy1-AF700 or –PerCPCy5.5 (clone 53–2.1). All antibodies were commercially purchased from Biolegend. For live/dead discrimination, a fixable viability dye, Zombie Aqua (Biolegend), was added to the surface antibody cocktail (diluted at 1:100). Cells were briefly fixed in 2% paraformaldehyde (PFA). Nucleated cells were identified by Draq5 stain (1:1000, Biolegend). Intracellular staining was performed using a fixation/permeabilization kit (BD Biosciences) according to manufac- turer's instructions. Intracellular antibodies for detection of Tuj1-AF647 or -AF488 (clone TUJ1, Biolegend), NeuN-PE (clone A60, Millipore Sigma), synaptophysin-AF488 (clone SY38, Millipore Sigma), and PSD- 95-APC (clone 6G6–1C9, Novus Biologicals) were incubated for 30 min at 4 °C and then washed.

Data were acquired on a BD LSRFortessa cytometer using FACSDiva 6.0 (BD Biosciences) and analyzed using FlowJo (Treestar Inc.). Absolute counting beads (Invitrogen) were used to estimate cell counts per the manufacturer's instructions. Neurons were identified as nucleated, singlet, live, $Thy1^{+}Tuj1^{+}NeuN^{+}$ cells. Resident microglia were identified as the $CD45^{int}$ $CD11b^{+}Ly6C^{-}$ population, whereas bone marrow-derived leukocytes were identified as $CD45^{hi}CD11b^{+}$ myeloid cells. Cell type-matched fluorescence minus one (FMO) controls were used to determine the positivity of each antibody. Prior to assessment on the cytometer, isolated cells were briefly probed to determine phagocytosis activity, oxidative stress level, autophagosome formation, and mitochondrial function as described below.

Phagocytosis was measured by incubating freshly isolated brain cells with 1-μm green fluorescent latex beads (1:500; Sigma) as described previously (Ritzel et al., 2015). In separate samples, cells were incubated for 1 h at 37 °C with pHrodo Red *E. coli* BioParticles (Invitrogen) according to the manufacturer's instructions. pHrodo Bio-particles are non-fluorescent outside of the cell but fluoresce brightly red in phagosomes. A separate study assessed ex vivo phagocytosis of myelin and apoptotic neurons. Briefly, YFP-positive neurons were isolated from the cortices of an adult SLICK transgenic mouse. The cells were then exposed to heat shock for 5 min at 60 °C, washed in HBSS, resuspended in RPMI, and kept on ice. Prior to assaying, the cell suspension was stained with FluoroMyelin Red (Thermo Fisher Scientific) according to the manufacturer's instructions. The cells were then washed, resuspended back in 5 mL of RPMI and placed on ice. Soon after, 50 μL of feeder cells were incubated with freshly isolated microglia for 45 min at 37 °C. Afterward, the cells were washed three times with 1 mL PBS.

Intracellular production of reactive oxygen species (e.g., peroxynitrite) was measured using dihydrorhodamine 123 (1:500; Invitrogen) as described previously (Ritzel et al., 2019). Mitochondrial dynamics were measured using MitoSpy Green and MitoSpy Red dyes (Biolegend) according to the company's protocol. LC3-associated autophagic vesicles were measured using the CYTO-ID Autophagy Detection Kit (Enzo Life Sciences) according to the manufacturer's instructions.

### 2.8. Statistical analysis

Quantitative data were plotted as mean ± standard error of the mean. Statistical analysis was performed using SigmaPlot Program, Version 12 (Systat Software) or GraphPad Prism software, version 4.00 for Windows (GraphPad Software, Inc). Statistical significance was evaluated between 2 individual samples using Student unpaired *t*-tests (detailed in figure legends). Comparisons within each surgery group were analyzed using two-way ANOVA with multiple comparisons test. For non-parametric data, Mann Whitney test was used. A $p$ value of $\leq 0.05$ was considered statistically significant.

# 3. Results

## 3.1. Timeline of behavioral testing for TBI mice

A battery of behavioral tests was evaluated, including the CatWalk, NOR, Y maze, TS, FST, nest building, social interaction, and sucrose preference tests, and were performed according to the schedule out-lined in Fig. 1.

## 3.2. Chronic TBI causes impairment in gait dynamics and cognition

Functional outcomes at late time points following experimental CCI injury in mice remain largely unexplored. To address this problem, we first examined gait dynamics at 26 weeks post-injury using the CatWalk apparatus, which measures the kinematic properties of locomotion. To evaluate overall motor coordination, regularity index, a parameter under the category of step sequencing, was selected. The result is a percentage of normal stepping that ideally reaches 100% in healthy animals(Hamers et al., 2001), though in practice, naive mice typically approach 90–100%. In response to TBI (Fig. 2A), the regularity index was significantly reduced to 87% ($N = 16$, $p \leq .05$) compared with Sham animals (92%, $N = 23$). The distance between the successive placement of the same paw, or stride length, was decreased in the right hind limb ($p \leq .05$, Fig. 2B), but not other limbs (Supplemental Fig. 1A–C). There are no apparent differences in the number of steps, average speed, or print position between sham and TBI groups (Supplemental Fig. 1D–F). However, the speed of the paw during swing phase, or swing speed, was also decreased in right-sided limb movement ($p \leq .05$, Fig. 2C). The distance between the position of the hind paw and the previously placed front paw, or print position, was significantly increased in right paws, indicating impaired range of motion ($p \leq .05$, Fig. 2D). The temporal relationship between placement of two paws (i.e., left front and right hind) within a step cycle, or phase dispersion, was ~2-fold higher after TBI, suggesting greater asynchrony in paw movements ($p \leq .01$, Fig. 2E). And lastly, coupling, which describes how movements of one leg are coupled to movements of the other leg, were significantly less synchronized after injury ($p \leq .05$, Fig. 2F). These findings imply that CCI injury results in chronic disruption of contralateral motor circuitry, unilaterally hampering locomotion.

Next we explored the long-term effects of TBI on cognitive behavior. Nesting behavior is essential for parental care and maintaining thermoregulation, and thus, can be considered an extended phenotype indicative of well-being. Although there was no difference in shredding, or weight change, of cotton squares after injury, the quality, or arrangement, of the nest site was significantly more unidentifiable ($p \leq .05$, Fig. 2G). Y maze testing at 26 weeks revealed a significant decrease in spontaneous alterations and no change in total entries, indicative of spatial working memory deficits ($p \leq .01$, Fig. 2H). Novel object recognition testing showed TBI mice spent comparably less time interacting with the novel object 24 h after the sample phase ($p \leq .001$, Fig. 2I). Given that sham and TBI mice spent equal time interacting with left- and right-side objects during the sample phase, our data suggest TBI induces lasting deficits in short-term recognition memory and preference for novelty (Fig. 2I). Taken together, our findings imply that CCI results in long-term cognitive impairment, which may impede daily activities crucial for survival such as nest building.

### 3.3. CCI causes depression and asocial behavior at 8 months post-injury

Major depression is considered a common sequel in TBI survivors. To investigate whether chronic TBI causes persistent changes in affect we implemented an array of tests to measure depressive-like behavior. Chronic TBI mice displayed greater immobility during tail suspension and forced swim tests at 27 weeks post-injury ($p \leq .01$ and $p \leq .05$, respectively; Fig. 3A–B). Compared to sham control, sucrose intake was significantly decreased in chronic TBI mice independent of water consumption or body weight, suggesting increased anhedonia ($p \leq .05$, Fig. 3C–I). To determine whether chronic TBI-induced depressive-like behavior is associated with changes in sociability we subjected mice to a three-chambered social interaction test. Both groups showed no baseline side preference when presented with empty cups in both chambers (Fig. 3J). Given the choice between an object (i.e., gray ball) or an age- and sex-matched mouse, both groups spent a similar amount of time interacting with the mouse rather than the object (Fig. 3K). However, when the object was replaced with a novel age- and sex- matched mouse, chronic TBI mice spent significantly less time interacting with the new mouse compared to sham mice, indicating decreased preference for social exploration ($p \leq .05$, Fig. 3L). Together, these data show that CCI causes marked depressive-like and social avoidant behaviors.

### 3.4. Chronic neurodegeneration is associated with changes in neuronal function

Flow cytometry has been used to purify selected cell types from brain tissue. To understand whether this technique could be used to ascertain neuronal health after TBI we utilized and validated a rapid, quantitative, high throughput procedure for measuring cellular function. To assess whether our simplified approach could identify living, nucleated, single cell neurons we used a combination of extracellular and intracellular labeling to probe for CD90 (Thy1), Beta-3 Tubulin (Tuj1), and NeuN expression. The nuclear dye, Draq5, was used to determine the scatter reference gate, and Zombie Aqua, an amine-reactive fluorescent viability dye, was used to determine the live/dead gate (Fig. 4A). Living, nucleated, single cells were then evaluated for expression of neuronal markers. Surface expression of Thy1 antibody was confirmed using SLICK-A (single-neuron labeling with inducible Cre-mediated knockout) transgenic mice which express EYFP under the Thy1 promoter (Fig. 4B) (Young et al., 2008). Because we observed differential expression of neuronal markers, we implemented a top- down gating strategy by sequentially gating based on expression pattern, starting from the most to least widely expressed markers (Fig. 4C). This approach provided the strongest confirmation that the cells in our gated population were definitive neurons.

To begin our analysis of the $Thy1^{+}Tuj1^{+}$ neuronal population, we performed an estimated cell count using absolute counting beads. The ipsilateral hemisphere of chronic CCI mice had significantly fewer neurons than sham controls, consistent with previous studies ($N = 5$/group, $p \leq .05$, Fig. 5A). The number and percentage of synaptophysin-and PSD-95-positive neurons were also significantly decreased after TBI, implying injury-induced diminishment in synaptic plasticity ($p \leq .05$, Fig. 5B–E). Neurons isolated from TBI mice showed increased expression of DHR123 relative to sham, indicating higher oxidative stress levels ($p \leq .05$, Fig. 5H–I). To examine other aspects of neuronal health we measured mitochondrial function using cell-permeant fluorogenic chemical reagents. Consistent with our viability

staining, all living neurons had functional mitochondria, however, fluorescent intensities were greater in neurons from injured mice ($p \leq .05$, Fig. 5J–K). To determine if increased mitochondrial activity was due to higher mitochondrial content we labeled cells with MitoSpy Green probe. Indeed, neurons from injured mice had greater mitochondrial mass than sham controls ($p \leq .05$, Fig. 5L–M). Lastly, to further highlight the utility of this approach to measuring neuronal function, we examined autophagic activity. Neurons from chronically injured mice showed higher frequencies LC3-positive autophagosome formation compared to sham mice, consistent with previous findings for acute time points ($p \leq .05$, Fig. 5F–G) (Sarkar et al., 2014). These findings support the use of flow cytometry for detecting changes in the disease state of injured neurons, and identify biomarkers of chronic TBI such as perturbations in mitochondrial dynamics and autophagy.

### 3.5. Chronic neurodegeneration is associated with a hyper-phagocytic phenotype and higher oxidative stress levels in microglia

Mechanisms of communication between neurons and microglia in the healthy brain maintain homeostatic activity. In TBI, these signaling pathways become disrupted often resulting in excessive microglia activation and chronic neuroinflammation. We thus characterized the cellular immune environment within the brain after 8 months CCI. An established gating strategy was employed to identify microglia and their peripheral counterparts in the brain (Fig. 6A). Significantly increased numbers of $CD45^{lo}CD11b^{+}$ microglia were found after TBI ($N = 5$/group, $p \leq .05$, Fig. 6B). Modest but significant increases in the engraftment of peripherally-derived $CD45^{hi}$ leukocyte populations were also found in the injured brain, implying mild chronic impairment in blood-brain barrier integrity ($p \leq .001$, Fig. 6C). The vast majority of these cells were putative lymphocytes, although bone marrow-derived myeloid populations ($CD45^{hi}CD11b^{+}$) were also significantly increased. Although no change in cell size was found, microglia granularity and oxidative stress level were statistically increased after TBI relative sham controls ($p \leq .05$, Fig. 6D–E, F–G), suggesting a heightened activation state.

Next, we examined phagocytic activity of microglia after TBI. While the frequency of microglia that had phagocytosed 1-$\mu m$ fluorescent latex beads showed a downward trend after injury, the percentage that phagocytosed *E. coli* bioparticles was significantly lower in the TBI brain ($p \leq .05$, Fig. 6L–M, P–Q). Surprisingly, the frequency of NeuN-positive microglia was significantly higher in TBI compared to sham control, indicating greater engulfment of neuronal debris ($p \leq .05$, Fig. 6N–O). To confirm this finding, we performed additional phagocytosis assays using fluorescently labeled myelin and apoptotic neurons. These data showed that TBI caused significantly increased uptake of both myelin and dying neurons up to one year after TBI (Supplemental Fig. 2A–B, C–D). Microglia from injured mice also showed greater formation of LC3-positive autophagosomes ($p \leq .001$, Fig. 6R–S). However, despite upward trends, no changes in mitochondrial content or membrane potential were seen (Fig. 6H–K). These results support the notion that microglial changes may play a role in synapse loss after chronic TBI and provide further evidence of differential impairment in cellular function that may contribute to neurological decline.

### 3.6. TBI causes chronic leukopenia and increased numbers of myeloid cells in the spleen

Finally, because changes in the systemic immune environment are becoming increasingly recognized as peripheral indicators of brain injury and functional outcome, we evaluated leukocyte counts in the blood and spleen of sham and chronic TBI mice. The number of circulating $CD45^+$ leukocytes were remarkably lower in chronic TBI mice, with comparably more striking decreases in $CD11b^+$ myeloid populations ($N = 8–10$/group, $p \leq .05$ and $p \leq .01$, respectively; Fig. 7A). Although no change in normalized spleen weight (data not shown) or total number of $CD45^+$ splenocytes or lymphocytes was found after injury, the number of $CD11b^+$ myeloid cells was substantially higher ($N = 5$/group, $p \leq .05$, Fig. 7B). In all, the compositional changes observed in the blood and spleen of TBI mice are consistent with chronic stress-induced leukopenia and extramedullary myelopoiesis, respectively.

## 4. Discussion

We show that a single moderate-level TBI has a profound and long- lasting impact on neurological outcome, characterized by depressive- like, cognitive and sensorimotor changes, as well as decreased preference for social novelty. These functional deficits coincided with TBI- associated changes in neuronal count, synaptic proteins, and oxidative stress level. Moreover, corresponding changes in microglia function, such as excessive phagocytic activity, support the notion that chronic microglial dysfunction may contribute to the chronic progressive neurodegeneration that are observed years after head injury. We also identify novel cellular markers of chronic brain injury using flow cytometry, including pathological alterations in the peripheral immune system. Together, these findings reinforce the idea that TBI alters the trajectory of normal aging, further compounding age-related neurological decline and immune pathology (Cole et al., 2015; Mouzon et al., 2018; Ritzel et al., 2018; Smith et al., 2013).

Due to the paucity of experimental TBI studies that employ very late time points, our understanding of the processes linking acute phase injury to late neurodegenerative pathology remains incomplete. We identify here a number of potentially important cellular changes 8 months after injury. Autophagosome formation in both neurons and microglia was significantly increased at eight months after CCI. Although defects in autophagic flux have been demonstrated during the acute phase of injury, it is not clear if that impairment persists, potentially accounting for disruptions in mitophagy or lysosomal clear- ance that may explain the increased production of reactive oxygen species and phagocytosis deficits found in this study (Sarkar et al., 2014; Wu and Lipinski, 2019).

Human TBI survivors often live for decades after the initial injury, many of whom experience cognitive deterioration and changes in mood state. To the extent that these behavioral phenotypes are both conserved and measurable in lower mammals, our study provides strong evidence that clinical signs of emotional dysregulation can be recapitulated in experimental chronic TBI. Relatively few experimental studies have investigated late effects of TBI (i.e., 6–12 months post-injury). While several studies to date have examined chronic outcomes in weight drop-impact acceleration and blast injury models of TBI (Ferguson et al., 2017; Rubenstein et al., 2019; Yin et al., 2014), the pathophysiology is distinct from CCI, which produces clear motor and cognitive deficits and accurate,

reproducible contusion injuries of graded severity (Xiong et al., 2013; Zhang et al., 2014). Using a widely applied and well-characterized mouse CCI model, we examined a variety of neurobehavioral changes and functional cellular alterations eight months after injury. This chosen injury duration of eight months is considered the human equivalent of ~40 years, marking the transition from young adulthood into middle age. There are, however, certain limitations to our study. First, mice were not repeatedly tested until 26 weeks, limiting our temporal understanding of these functional outcomes. Thus, whether these changes reflect the peak or ceiling for each deficit, or rather, a gradual return to baseline remains unclear. However, by leaving the mice unperturbed for this entire length of time, our data were not confounded by repeated handling or experimenter-induced stress on the animal. Another potential caveat is that stressful tests such as tail suspension and forced swim could carry over and negatively influence subsequent testing behavior. Although we cannot rule this out, these depression tests were only performed once and a rest period of 1–2 weeks was scheduled prior to the analysis of nest construction and social preference, two relatively low-stress tests. Interestingly, the fact that TBI mice exhibited greater behavioral deficits in these tests compared to sham control mice suggests that the effects of ‘test-induced stress’ compound TBI injury, which is in line with the behavioral dysfunction observed in nearly all other tests. It is noteworthy too that TBI survivors report higher long-term prevalence of anxiety disorders and post-traumatic stress disorder (Kaplan et al., 2018; Osborn et al., 2017; Scholten et al., 2016). Nevertheless, the behavioral assessments performed in this study were well powered to examine potential changes across tests.

Our behavioral characterization of the chronic TBI model provides one of the most extensive and diverse assessments to date. For example, this was the first study to demonstrate chronic deficits in gait dynamics following TBI. Walking requires central integration and processing of somatosensory, visual, and vestibular sensory afferents. The data show that chronic TBI causes unilateral alterations in gait performance that would be predicted based on the position of the impact site. This is consistent with an earlier study which found spontaneous forelimb preference (i.e., asymmetry) up to 5 months after CCI (Baskin et al., 2003). Previous work demonstrated that 12 months after experimental TBI in Rhesus monkeys, chronic inflammation in the motor cortex extends to the corticospinal tract in the spinal cord (Nagamoto-Combs et al., 2007). Lasting deficits in balance and coordination have been shown in mice up to one year after CCI (Shear et al., 2004). However, this impairment was only evident when the rotations per minute (rpm) were increased from 5 to 20 in the rotarod test.

Nearly half of all TBI survivors experience depression within the first year, and nearly two-thirds are affected within seven years (Fann et al., 2009; Hibbard et al., 1998; Jorge et al., 2004). Because TBI is more prevalent in young adults, the lifetime risk of depressive complications is of serious concern. Our findings are consistent with the proposed link between depression and chronic inflammation (Bodnar et al., 2018; Pape et al., 2019). A recent study reported decreased socialization and decreased mobility in the tail suspension test at 6 months after CCI (Davies et al., 2018). Our findings support these observations and provide additional context. The total number of microglia was significantly higher in the chronic TBI brain, with the influx or engraftment of peripheral myeloid cells modest but evident. The regional distribution of these bone marrow-derived cells is unknown, but

imply increased permissiveness of the chronic TBI brain to leukocyte infiltration likely via site-specific disruptions in blood-brain barrier integrity (Soto et al., 2015).

Functionally, we provide extensive evidence for TBI-induced dysregulation of microglia phagocytosis. The inability to clear debris is thought to precipitate plaque deposition and age-related neurodegenerative disease (Galloway et al., 2019). Given that previous work has shown reduced thickness in the corpus collosum, gliosis, and higher APP-immunoreactivity, impairment in debris clearance may underlie the worsened outcomes seen in APP/PSI transgenic mice at 8 months after experimental TBI (Cheng et al., 2019; Mouzon et al., 2018). Our finding that chronic CCI enhances microglial engulfment of dying neurons and myelin, however, offers an alternative explanation. The hyper-phagocytic phenotype seen in our study is consistent with that reported in other mouse models of neurodegeneration, and suggests that chronic microglia activation may be linked to excessive synaptic pruning or synapse loss (Henstridge et al., 2019; Rajendran and Paolicelli, 2018). This idea is supported by the decreased expression of synaptic proteins in living neurons of injured mice. The mechanism underlying this hyperactive phagocytic activity is not clear. Interestingly, a recent transcriptomic study reported increased brain expression of complement factors and impaired synaptic function as late as one year post-TBI (Boone et al., 2019). Although oxidative stress levels were also higher in microglia after chronic TBI, changes were less than reported during the initial days of injury (Ritzel et al., 2019). Nevertheless, elevated ROS production and perturbations in autophagic function are supported by our previous work, which demonstrated that microglia activation persists for up to one year post-CCI and is associated with greater NOX2 and CD68-immunoreactivity, respectively (Loane et al., 2014).

Currently, most studies to date have centered on characterizing the fundamental changes in neurological impairment and brain pathology. The current study adds to this growing body of knowledge by identifying novel targets of cellular and molecular dysfunction using a new method of assessing TBI pathology (i.e., flow cytometry). It is important to note that the present study is phenomenological in nature and does not address causation. Histological validation of neuronal or microglia counts in brain regions such as the amygdala would provide key spatial information regarding the anatomical underpinnings of depressive-like behavior. Future studies are required to address the structure-function relationship of brain trauma, including the anatomical correlates of chronic anxiety and depression.

Stereological methods of cell counting using histological staining techniques are considered the gold standard for measuring neuronal loss and lesion volume. Histology embraces the study of the structures of both tissue and cells, and the relationship between these structures and physiological function. Yet, no method is without limitation. For example, tissue artifacts may result from a number of causes including improper fixation, dehydration, cryopreservation, storage temperature, humidity, reagents, or poor microtome sectioning. Because the tissue is fixed, the data capture a static rather than dynamic snapshot of neuropathology. Moreover, tissue fixation can render epitopes inaccessible to antibody recognition (i.e., epitope masking), making it difficult to troubleshoot immunofluorescence staining for some biomarkers. As an alternative approach, ‘neurocytometry’ is highly quantitative and lends itself to the measurement and probing of living neurons, providing

a dynamic window into the cellular behavior and molecular processes that go awry in TBI. For example, we observed a decrease in the number of living neurons after TBI, consistent with earlier histopathological analyses from our laboratory and others (Campos-Pires et al., 2019; Loane et al., 2014). In addition, flow cytometry experiments can be performed and analyzed in the same day. Neurocytometry is not without its own limitations, particularly with regard to cellular activation due to the mechanical and enzymatic digestion process. Garnering spatial information like mapping cytoarchitectural changes or making volumetric measurements of lesion size is also not possible. However, a growing body of evidence suggests that it can and should be considered for certain neuroscience applications.

The neurocytometry protocol detailed here has the potential to enhance our understanding of neuronal function in health and injury, and may significantly expand TBI studies to assess a multitude of cellular changes without the requirement for in situ fixation, allowing for additional analysis of leftover cells or tissue (Benoit et al., 2018; Berl et al., 2017; Guez-Barber et al., 2012; Legroux et al., 2015; Lobo et al., 2006; Martin et al., 2017; Sergent-Tanguy et al., 2003; Yamasaki et al., 2018). The initial gating steps that determine whether the putative neuron is a single, nucleated, living cell are crucial, as this simple high-throughput procedure generates a high level of cellular debris that can obfuscate analysis. Several studies use myelin removal kits to reduce debris. However helpful, we find that this step is not necessary. Instead, the identification of a stable forward- versus side-scatter (FSC/SSC) reference gate is essential for eliminating the vast majority of non-cellular events from subsequent gating steps. This can be determined using a combination of fluorogenic nuclear dyes, viability stains, and neuronal markers. Nonetheless, collection and analysis can be slow and tedious due to large amounts of debris; however, this can be partially circumvented using a FSC/SSC storage gate. It was also noted that the addition of EDTA during the enzymatic digestion and prior to fixation or collection is essential for papain activation and preventing cell clumping (i.e., doublets), respectively. Importantly, this neurocytometry approach can be exploited using any fluorogenic dye or conjugated antibody to measure a target function or biomarker.

We extended our flow cytometric analysis of immune cells to include neurons in an effort to enhance our understanding of TBI-induced alterations in neuronal activity, which is not easily measured by immunohistochemistry due to fixation requirements. The rapid isolation of these cells, although likely to induce some degree of activation or death itself, allows researchers the opportunity to evaluate neuronal activity ex vivo within a short time window after sacrifice, preserving many aspects their in vivo functional identity. The number of living neurons evaluated in each experiment can be adjusted as necessitated, but generally fall within the range of values obtained by standard histological counting (Collins et al., 2010). To date, the vast majority of chronic (e.g., > 6 months) TBI studies in mice have centered on the quantification of neuronal death or lesion volume, rather than probing for changes in cellular function of living neurons. Our data support the use of flow cytometry for rapid analysis of neuronal counts and function in brain injury, and can be further optimized to enrich for select populations. Future studies will be required to understand the spatio- temporal progression of TBI-mediated changes in cellular function.

## 5. Conclusion

These experimental findings reveal that chronic TBI is associated with diverse neurobehavioral deficits and associated functional changes in neurons and microglia. TBI-driven changes in cellular function can be characterized by flow cytometry and help clarify our understanding of the pathogenesis of posttraumatic neurodegeneration.

The following are the supplementary data related to this article.

## Supplementary Material

Refer to Web version on PubMed Central for supplementary material.

## Acknowledgements

We thank Dr. Bogdan Stoica for generously providing us with the SLICK-A mice. We thank Ms. Lulu Liu for expert technical support. This study was supported by the National Institute of Neurological Disorders and Stroke for R01 NS094527 (JW), R01 NS110635 (JW/AIF), R01 NS110567 (JW), F32 NS105355 (RMR), the National Institute of Nursing Research for 2R01 NR013601 (JW/AIF), and the National Institute on Aging for RF1 NS110637 (JW).

## References

Baskin YK, et al. , 2003. Two effective behavioral tasks for evaluating sensorimotor dysfunction following traumatic brain injury in mice. J. Neurosci. Methods 129, 87–93. [PubMed: 12951236]

Benoit A, et al. , 2018. Flow cytometry for receptor analysis from ex-vivo brain tissue in adult rat. J. Neurosci. Methods 304, 11–23. [PubMed: 29660368]

Berl S, et al. , 2017. Enrichment and isolation of neurons from adult mouse brain for ex vivo analysis. J. Neurosci. Methods 283, 15–22. [PubMed: 28336359]

Bodnar CN, et al. , 2018. Depression following a traumatic brain injury: uncovering cytokine dysregulation as a pathogenic mechanism. Neural Regen. Res. 13, 1693–1704. [PubMed: 30136679]

Boone DR, et al. , 2019. Traumatic brain injury induces long-lasting changes in immune and regenerative signaling. PLoS One 14, e0214741.

Campos-Pires R, et al. , 2019. Xenon improves long-term cognitive function, reduces neuronal loss and chronic neuroinflammation, and improves survival after traumatic brain injury in mice. Br. J. Anaesth. 123, 60–73. [PubMed: 31122738]

Cheng WH, et al. , 2019. CHIMERA repetitive mild traumatic brain injury induces chronic behavioural and neuropathological phenotypes in wild-type and APP/PS1 mice. Alzheimers Res. Ther 11, 6. [PubMed: 30636629]

Cole JH, et al. , 2015. Prediction of brain age suggests accelerated atrophy after traumatic brain injury. Ann. Neurol. 77, 571–581. [PubMed: 25623048]

Collins CE, et al. , 2010. A rapid and reliable method of counting neurons and other cells in brain tissue: a comparison of flow cytometry and manual counting methods. Front. Neuroanat. 4, 5. [PubMed: 20300202]

Crane PK, et al. , 2016. Association of traumatic brain injury with late-life neurode-generative conditions and neuropathologic findings. JAMA Neurol. 73, 1062–1069. [PubMed: 27400367]

Cruz-Haces M, et al. , 2017. Pathological correlations between traumatic brain injury and chronic neurodegenerative diseases. Transl. Neurodegener. 6, 20. [PubMed: 28702179]

Davies M, et al. , 2018. Delayed hypoxemia after traumatic brain injury exacerbates long-term behavioral deficits. J. Neurotrauma 35, 790–801. [PubMed: 29149808]

Deacon RM, 2006. Assessing nest building in mice. Nat. Protoc. 1, 1117–1119. [PubMed: 17406392]

DeKosky ST, Asken BM, 2017. Injury cascades in TBI-related neurodegeneration. Brain Inj. 31, 1177–1182. [PubMed: 28981345]

Fann JR, et al. , 2009. Treatment for depression after traumatic brain injury: a systematic review. J. Neurotrauma 26, 2383–2402. [PubMed: 19698070]

Ferguson S, et al. , 2017. Acute or delayed treatment with Anatabine improves spatial memory and reduces pathological Sequelae at late time-points after repetitive mild traumatic brain injury. J. Neurotrauma 34, 1676–1691. [PubMed: 27889957]

Galloway DA, et al. , 2019. Phagocytosis in the brain: homeostasis and disease. Front. Immunol. 10, 790. [PubMed: 31040847]

Guez-Barber D, et al. , 2012. FACS purification of immunolabeled cell types from adult rat brain. J. Neurosci. Methods 203, 10–18. [PubMed: 21911005]

Hamers FP, et al. , 2001. Automated quantitative gait analysis during overground locomotion in the rat: its application to spinal cord contusion and transection injuries. J. Neurotrauma 18, 187–201. [PubMed: 11229711]

Hay J, et al. , 2016. Chronic traumatic encephalopathy: the neuropathological legacy of traumatic brain injury. Annu. Rev. Pathol. 11, 21–45. [PubMed: 26772317]

Henstridge CM, et al. , 2019. Glial contribution to excitatory and inhibitory synapse loss in neurodegeneration. Front. Cell. Neurosci. 13, 63. [PubMed: 30863284]

Hibbard MR, et al. , 1998. Undiagnosed health issues in individuals with traumatic brain injury living in the community. J. Head Trauma Rehabil. 13, 47–57. [PubMed: 9651239]

Johnson VE, et al. , 2017. Traumatic brain injury as a trigger of neurodegeneration. Adv Neurobiol. 15, 383–400. [PubMed: 28674990]

Jorge RE, et al. , 2004. Major depression following traumatic brain injury. Arch. Gen. Psychiatry 61, 42–50. [PubMed: 14706943]

Kaplan GB, et al. , 2018. Pathophysiological bases of comorbidity: traumatic brain injury and post-traumatic stress disorder. J. Neurotrauma 35, 210–225. [PubMed: 29017388]

Legroux L, et al. , 2015. An optimized method to process mouse CNS to simultaneously analyze neural cells and leukocytes by flow cytometry. J. Neurosci. Methods 247, 23–31. [PubMed: 25819540]

Loane DJ, et al. , 2014. Progressive neurodegeneration after experimental brain trauma: association with chronic microglial activation. J. Neuropathol. Exp. Neurol. 73, 14–29. [PubMed: 24335533]

Lobo MK, et al. , 2006. FACS-array profiling of striatal projection neuron subtypes in juvenile and adult mouse brains. Nat. Neurosci. 9, 443–452. [PubMed: 16491081]

Martin D, et al. , 2017. Neurocytometry: flow cytometric sorting of specific neuronal populations from human and rodent brain. ACS Chem. Neurosci. 8, 356–367. [PubMed: 28135061]

Masel BE, DeWitt DS, 2010. Traumatic brain injury: a disease process, not an event. J. Neurotrauma 27, 1529–1540. [PubMed: 20504161]

Matyas JJ, et al. , 2017. Truncated TrkB.T1-mediated astrocyte dysfunction contributes to impaired motor function and neuropathic pain after spinal cord injury. J. Neurosci. 37, 3956–3971. [PubMed: 28270575]

Mouzon BC, et al. , 2014. Chronic neuropathological and neurobehavioral changes in a repetitive mild traumatic brain injury model. Ann. Neurol. 75, 241–254. [PubMed: 24243523]

Mouzon BC, et al. , 2018. Lifelong behavioral and neuropathological consequences of repetitive mild traumatic brain injury. Ann. Clin. Transl. Neurol. 5, 64–80. [PubMed: 29376093]

Moy SS, et al. , 2004. Sociability and preference for social novelty in five inbred strains: an approach to assess autistic-like behavior in mice. Genes Brain Behav. 3, 287–302. [PubMed: 15344922]

Nagamoto-Combs K, et al. , 2007. Prolonged microgliosis in the rhesus monkey central nervous system after traumatic brain injury. J. Neurotrauma 24, 1719–1742. [PubMed: 18001202]

Nakagawa Y, et al. , 1999. Traumatic brain injury in young, amyloid-beta peptide overexpressing transgenic mice induces marked ipsilateral hippocampal atrophy and diminished Abeta deposition during aging. J. Comp. Neurol. 411, 390–398. [PubMed: 10413774]

Osborn AJ, et al. , 2017. Anxiety and comorbid depression following traumatic brain injury in a community-based sample of young, middle-aged and older adults. J. Affect. Disord. 213, 214–221. [PubMed: 27919428]

Osier ND, et al. , 2015. Chronic Histopathological and Behavioral outcomes of experimental traumatic brain injury in adult male animals. J. Neurotrauma 32, 1861–1882. [PubMed: 25490251]

Pape K, et al. , 2019. Immunoneuropsychiatry - novel perspectives on brain disorders. Nat. Rev. Neurol. 15, 317–328. [PubMed: 30988501]

Piao CS, et al. , 2013. Late exercise reduces neuroinflammation and cognitive dysfunction after traumatic brain injury. Neurobiol. Dis. 54, 252–263. [PubMed: 23313314]

Popescu C, et al. , 2015. Actual data on epidemiological evolution and prevention en- deavours regarding traumatic brain injury. J. Med. Life. 8, 272–277. [PubMed: 26351526]

Raj R, et al. , 2017. Risk of hospitalization with neurodegenerative disease after moderate-to-severe traumatic brain injury in the working-age population: a retrospective cohort study using the Finnish national health registries. PLoS Med. 14, e1002316.

Rajendran L, Paolicelli RC, 2018. Microglia-mediated synapse loss in Alzheimer's disease. J. Neurosci. 38, 2911–2919. [PubMed: 29563239]

Ritzel RM, et al. , 2015. Age- and location-related changes in microglial function. Neurobiol. Aging 36, 2153–2163. [PubMed: 25816747]

Ritzel RM, et al. , 2018. Chronic alterations in systemic immune function after traumatic brain injury. J. Neurotrauma 35, 1419–1436. [PubMed: 29421977]

Ritzel RM, et al. , 2019. Old age increases microglial senescence, exacerbates secondary neuroinflammation, and worsens neurological outcomes after acute traumatic brain injury in mice. Neurobiol. Aging 77, 194–206. [PubMed: 30904769]

Rubenstein R, et al. , 2019. Novel mouse tauopathy model for repetitive mild traumatic brain injury: evaluation of long-term effects on cognition and biomarker levels after therapeutic inhibition of tau phosphorylation. Front. Neurol. 10, 124. [PubMed: 30915013]

Sarkar C, et al. , 2014. Impaired autophagy flux is associated with neuronal cell death after traumatic brain injury. Autophagy. 10, 2208–2222. [PubMed: 25484084]

Scholten AC, et al. , 2016. Prevalence of and risk factors for anxiety and depressive disorders after traumatic brain injury: a systematic review. J. Neurotrauma 33, 1969–1994. [PubMed: 26729611]

Sergent-Tanguy S, et al. , 2003. Fluorescent activated cell sorting (FACS): a rapid and reliable method to estimate the number of neurons in a mixed population. J. Neurosci. Methods 129, 73–79. [PubMed: 12951234]

Shear DA, et al. , 2004. Neural progenitor cell transplants promote long-term functional recovery after traumatic brain injury. Brain Res. 1026, 11–22. [PubMed: 15476693]

Smith DH, et al. , 2013. Chronic neuropathologies of single and repetitive TBI: substrates of dementia? Nat. Rev. Neurol. 9, 211–221. [PubMed: 23458973]

Soto I, et al. , 2015. APOE stabilization by exercise prevents aging neurovascular dysfunction and complement induction. PLoS Biol. 13, e1002279.

Taylor CA, et al. , 2017. Traumatic brain injury-related emergency department visits, hospitalizations, and deaths - United States, 2007 and 2013. MMWR Surveill. Summ. 66, 1–16.

Wojnarowicz MW, et al. , 2017. Considerations for experimental animal models of concussion, traumatic brain injury, and chronic traumatic encephalopathy-these matters matter. Front. Neurol. 8, 240. [PubMed: 28620350]

Wu J, Lipinski MM, 2019. Autophagy in Neurotrauma: good, bad, or dysregulated. Cells. 8.

Wu J, et al. , 2014. Spinal cord injury causes brain inflammation associated with cognitive and affective changes: role of cell cycle pathways. J. Neurosci. 34, 10989–11006. [PubMed: 25122899]

Wu J, et al. , 2016. Endoplasmic reticulum stress and disrupted neurogenesis in the brain are associated with cognitive impairment and depressive-like behavior after spinal cord injury. J. Neurotrauma 33, 1919–1935. [PubMed: 27050417]

Xiong Y, et al. , 2013. Animal models of traumatic brain injury. Nat. Rev. Neurosci. 14, 128–142. [PubMed: 23329160]

Yamasaki T, et al. , 2018. Flow Cytometric detection of PrP(Sc) in neurons and glial cells from prion-infected mouse brains. J. Virol. 92.

Yin TC, et al. , 2014. P7C3 neuroprotective chemicals block axonal degeneration and preserve function after traumatic brain injury. Cell Rep. 8, 1731–1740. [PubMed: 25220467]

Young P, et al. , 2008. Single-neuron labeling with inducible Cre-mediated knockout in transgenic mice. Nat. Neurosci. 11, 721–728. [PubMed: 18454144]

Zaloshnja E, et al. , 2008. Prevalence of long-term disability from traumatic brain injury in the civilian population of the United States, 2005. J. Head Trauma Rehabil. 23, 394–400. [PubMed: 19033832]

Zhang YP, et al. , 2014. Traumatic brain injury using mouse models. Transl. Stroke Res. 5, 454–471. [PubMed: 24493632]

Zhao Z, et al. , 2012. Comparing the predictive value of multiple cognitive, affective, and motor tasks after rodent traumatic brain injury. J. Neurotrauma 29, 2475–2489. [PubMed: 22924665]

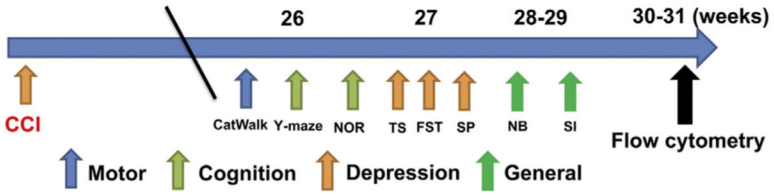


**Fig. 1.**

Behavioral test schedule.

The CatWalk, Y-maze, and novel object recognition (NOR) task were performed at 26-weeks post-injury. The tail-suspension (TS), forced swim test (FST), and sucrose preference (SP) tests were performed at 27-weeks post-injury. The nesting building (NB) and social interaction (SI) tests were conducted at 28–29- weeks post-injury. On weeks 30–31, all of the mice were euthanized and per- fused for flow cytometry. Abbreviation: CCI cortical impact injury.

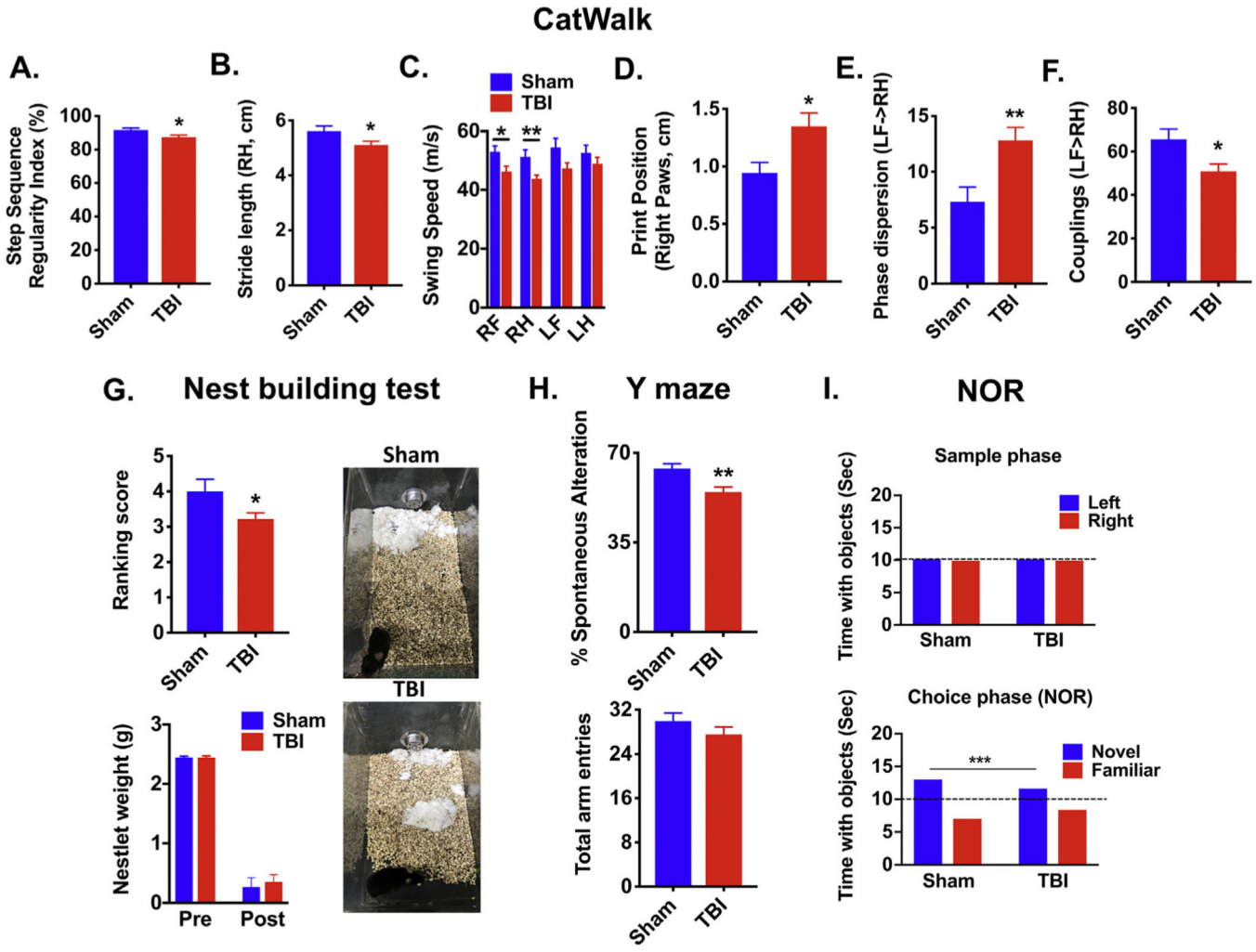


**Fig. 2.**

Experimental TBI causes lasting disturbances in gait dynamics and cognitive memory impairment.

Gait analysis was performed on C57BL/6 male mice using the CatWalk apparatus at 26 weeks post-injury ($N$ = 16–23/group). The primary variables analyzed are shown and defined in the main text. These parameters include step sequence regularity index (A), stride length of right hind limbs (B), swing speed (C), print position of right paws (D), and phase dispersion (E) and couplings (F) of the left front and right hind limbs. Gait parameters were analyzed by Student's unpaired $t$-test or two- way ANOVA with multiple comparison analysis. The ability to perform activities of daily living such as nest construction, an indicator of well being, was measured at 28 weeks post-injury (N = 16–23/group). Differences in the quality and appearance of constructed nest sites were evident after TBI, independent of the weight change in the cotton nestlet (Mann-Whitney test; G). Representative images illustrate that nestlets in individually-housed TBI mouse cages were mostly shredded but often showed no identifiable nest site, whereas nestlets in sham mouse cages were identifiable but flat nest with > 90% of the nestlet torn. Short-term spatial working memory was tested at 26 weeks post-injury using Y-maze (N = 16–23/group).

TBI-mediated changes in the percentage of spontaneous alterations and total number of arm entries are shown (H). Novel object recognition (NOR) task was performed at 26-weeks post-injury (N = 16–23/group). No difference in the amount time spent with the object was seen during the sample phase, whereas, TBI mice spent significantly less time with the novel object during the choice phase (I). Error bars show mean SEM. Abbreviation: RH right hind, LF left front, g grams, cm centimeters, *sec* seconds, TBI traumatic brain injury, SEM standard error of mean. *p < .05, **p < .01, and ***$p$ < .001.

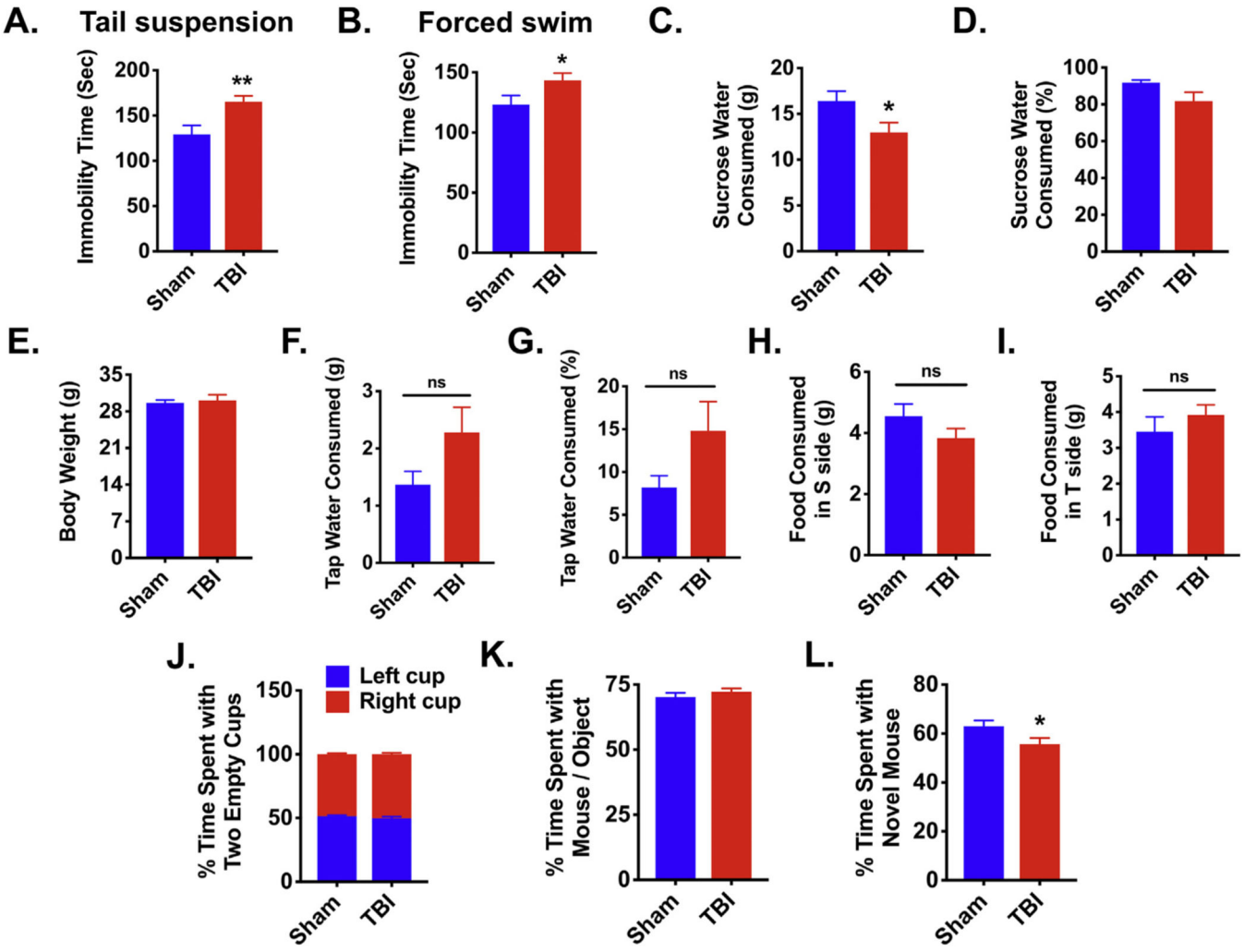


**Fig. 3.**

Increased depressive-like phenotypes and asocial behavior are evident in chronic TBI mice. Tail suspension, forced swim, and sucrose consumption tests for depressive-like behaviors were performed at 27 weeks post-injury. For all behavioral experiments, N = 16–23/group. TBI mice exhibited greater immobility in the tail suspension test (A) and forced swim test (B) as determined by Student's unpaired *t*-test. TBI mice consumed fewer grams of sucrose water compared to sham mice (C). No change was seen in the percentage of sucrose water consumed (D), body weight (E), grams of tap water consumed (F), percentage of tap water consumed (G), grams of food consumed in the S side (H), or grams of food consumed in the T side (I). The social interaction test was conducted at 29 weeks post-injury. Both groups spent a similar amount of time with the left and right cup (J) and with an age- and sex-matched mouse and an object (i.e., gray ball) (K). When the object was replaced with a novel age- and sex-matched mouse, TBI mice spent significantly less time interacting with the novel mouse as compared to sham mice (L). Error bars show mean SEM. Abbreviation: g grams, sec seconds, ns not significant, s sucrose, t tap water, TBI traumatic brain injury, SEM standard error of mean. *p < .05 and **p < .01.

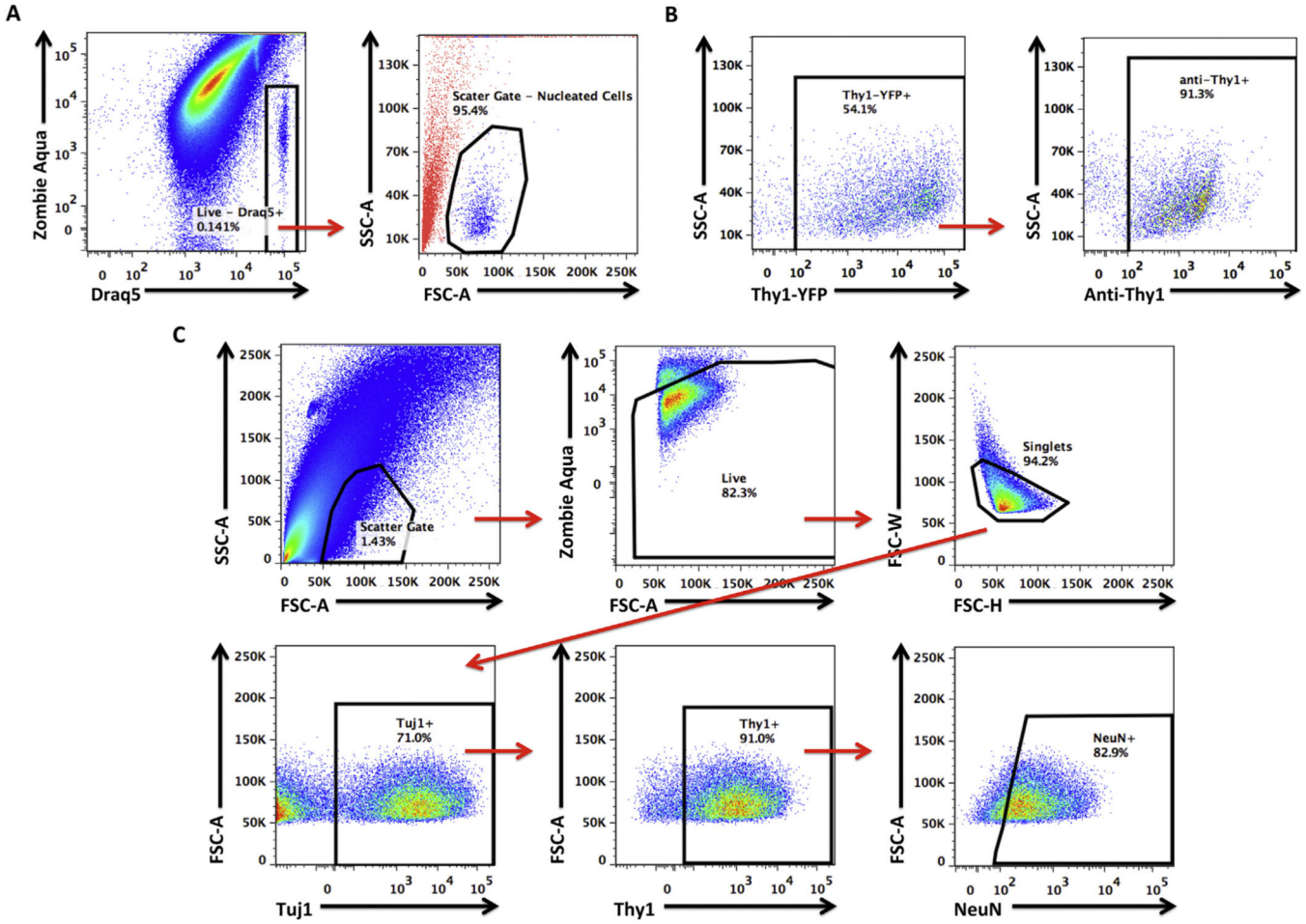


**Fig. 4.**

Gating strategy for identifying neuronal populations in the brain using flow cytometry. Representative dot plots show the identification of living, nucleated cells in single cell suspensions of brain tissue, based on Zombie Aqua and Draq5 staining pattern (A). Using a backgating approach, we show that this population of living, nucleated cells (in blue) have specific side- and forward-scatter features that distinguish them from all other non-cellular events or debris (in red). To confirm the specificity of our neuronal labeling strategy using a fluorophore-conjugated anti-Thy1 antibody, we validated its use in SLICK-A transgenic mice, which express EYFP under the control of the Thy1 promoter and serve as a fluorescent reporter of cortical neurons. Representative dot plots illustrate that anti-Thy1 antibody conjugated to AF700 stained greater than ~90% of all $EYFP^+$ SLICK-A cortical neurons (B). After confirming the scatter reference gate for living, nucleated cells and validating the neuronal marker anti-Thy1, we determined the specificity of our neuronal gating strategy using the neuronal markers Tuj1 and NeuN (C). A consistently large percentage (i.e., ~70%) of living, nucleated, single cells (i.e., singlets) were $Tuj1^+$, of which the vast majority co-expressed Thy1. A high proportion of $Tuj1^+Thy1^+$ cells also stained positive for NeuN. The illustrated gating strategy provided confirmation that the identified cells were living neurons. Abbreviation: SSC-A side scatter-area, FSC-A forward scatter-area, FSC-W forward scatter-width, FSC-H forward scatter-height.

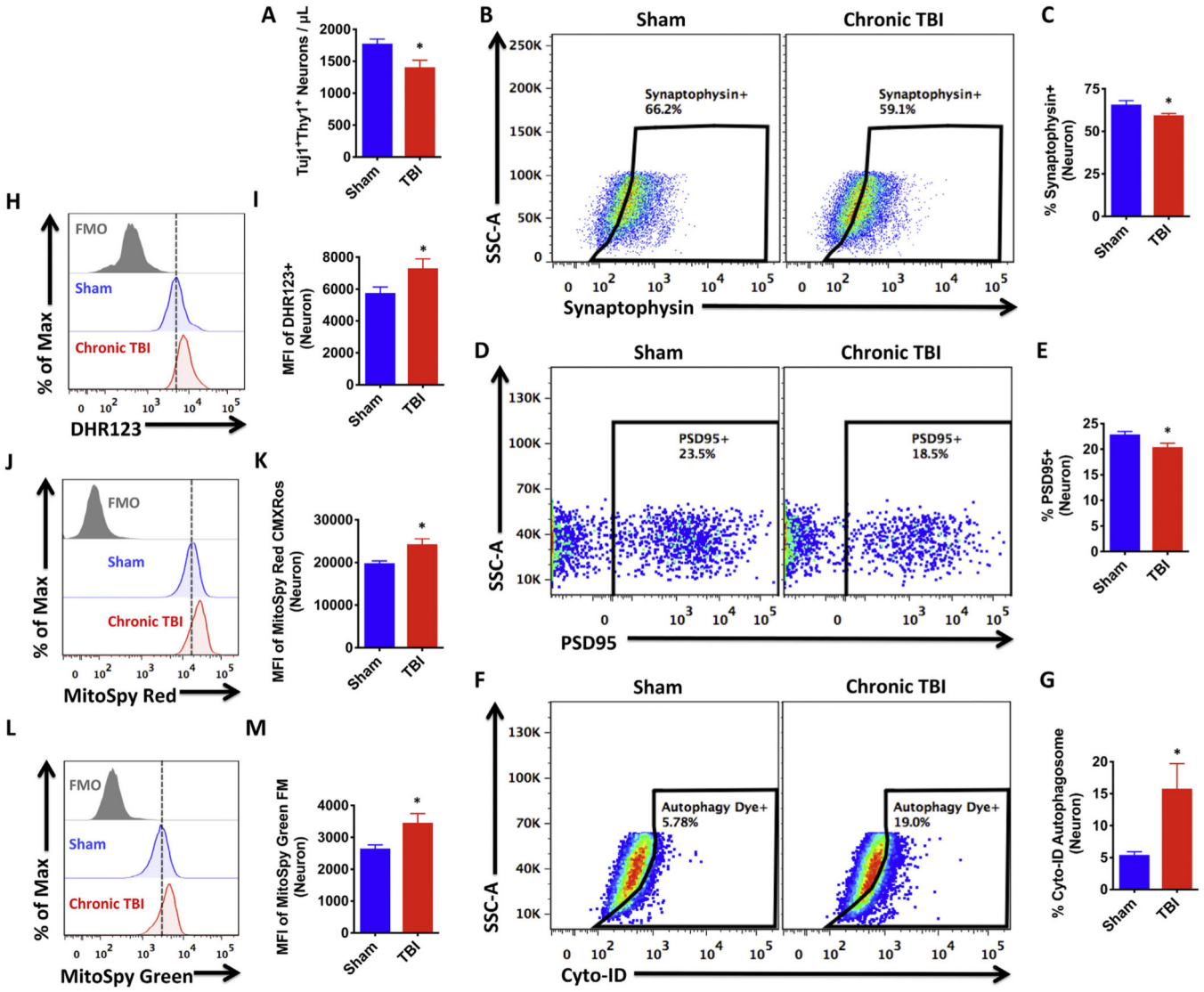


**Fig. 5.**

TBI chronically alters neuronal function.

Living Tuj1$^{+}$Thy1$^{+}$ neuronal counts in the ipsilateral hemisphere of sham and chronic TBI mice were estimated using counting beads (Student's unpaired *t*-test; A). Representative dot plots illustrate intracellular staining for synaptophysin in neurons (B). The frequency of synaptophysin-positive neurons was quantified (C). Representative dot plots depict intracellular staining for PSD-95 in sham and chronic TBI neurons (D). The frequency of PSD-95-positive neurons was quantified (E). Autophagic vesicles were measured using Cyto-ID dye. Representative dot plots show the percentage of autophagosome-positive neurons in sham and TBI groups (F). Quantification of autophagosome-positive neurons is shown (G). Oxidative stress was measured using DHR123 and the relative level of reactive oxygen species production by the Tuj1$^{+}$Thy1$^{+}$ neuronal population is shown in the representative histogram (H). MFI quantification of DHR123-positive neurons is shown (I). Mitochondrial membrane potential was measured using MitoSpy Red CMXRos and the relative level of mitochondrial function in neurons is depicted in the

re presentative histogram (J). MFI quantification of MitoSpy Red-positive neurons is shown (K). Mitochondrial mass was measured using MitoSpy Green FM and the relative level of mitochondrial content in neurons is depicted in the representative histogram (L). MFI quantification of MitoSpy Green-positive neurons is shown (M). For all experiments, $N = 5$/group. Error bars show mean SEM. Abbreviation: FMO fluorescence minus one control, MFI mean fluorescence intensity, DHR123 dihydrorhodamine 123, Max maximum, SSC-A side scatter-area, TBI traumatic brain injury, SEM standard error of mean. *$p < .05$.

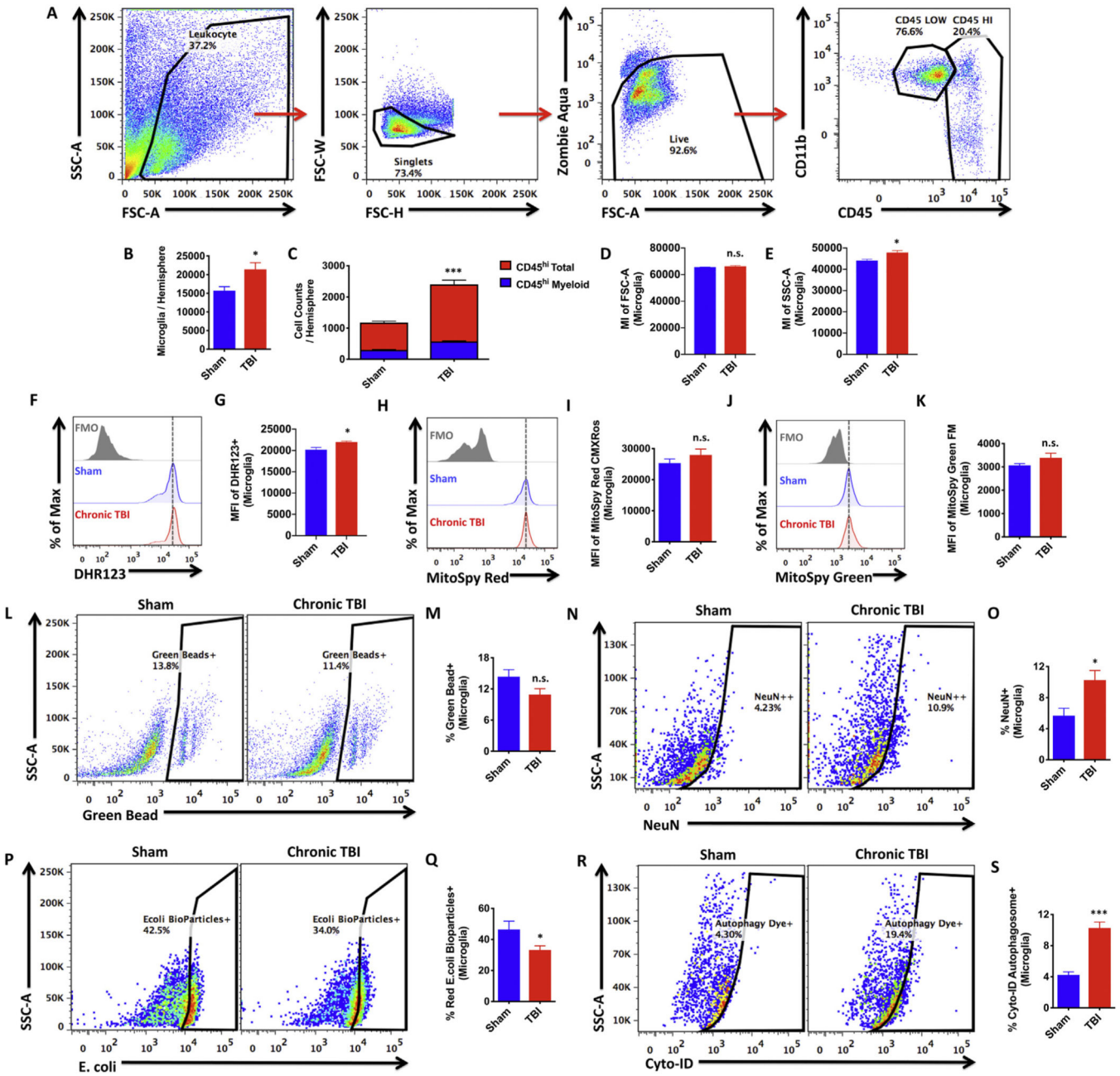


**Fig. 6.**

TBI chronically alters microglia function.

Microglia activation in the ipsilateral hemisphere of sham and TBI mice was evaluated at 8 months post-injury. The gating strategy for microglial identification is depicted (A). Higher numbers of $CD45^{lo}CD11b^{+}$ microglia were found in the TBI brain compared to sham controls as determined by Student's unpaired t-test (B). Higher numbers of $CD45^{hi}$ peripheral leukocytes were found in the TBI brain relative sham (C). Putative lymphocyte populations ($CD45^{hi}CD11b^{-}$, in red) represent the predominant leukocyte found in the brain at 8 months post-injury. The mean intensities for FSC-A and SSC-A of microglia are shown for both groups (D and E, respectively). Oxidative stress was measured using DHR123 and

the relative level of reactive oxygen species production by microglia is illustrated in the re- presentative histogram (F). MFI quantification of DHR123-positive microglia is shown (G). Mitochondrial membrane potential was measured using MitoSpy Red CMXRos and the relative level of mitochondrial function is illustrated in the representative histogram (H). MFI quantification of MitoSpy Red-positive microglia is shown (I). Mitochondrial mass was measured using MitoSpy Green FM and the relative level of mitochondrial content is depicted in the representative histogram (J). MFI quantification of MitoSpy Green-positive microglia is shown (K). Microglial phagocytosis was measured using 1-μm green fluorescent latex beads, red pHrodo *E.coli* bioparticles, and intracellular NeuN, a neuronal marker. A representative dot plot depicts the percentage of green bead-positive microglia (L). Quantification of bead-positive phagocytic microglia is shown (M). The presence of intracellular NeuN protein was measured (N). The percentage of NeuN-positive microglia was quantified (O). A representative dot plot depicts the percentage of microglia containing *E.coli* bioparticles inside phagosomes (P). The frequency of *E.coli*-positive phagocytic microglia is shown (Q). Autophagic vesicles were measured using Cyto-ID dye. Representative dot plots show the percentage of LC3-associated autop- hagosome-positive microglia in sham and chronic TBI groups (R). Quantification of autophagosome-positive microglia is shown (S). For all experiments, N = 5/ group. Error bars show mean SEM. Abbreviation: MI mean intensity, MFI mean fluorescence intensity, DHR123 dihydrorhodamine 123, Max maximum, SSC-A side scatter-area, FSC-A forward scatter-area, FSC-W forward scatter-width, FSC-H forward scatter-height, FMO fluorescence minus one control, ns not significant, TBI traumatic brain injury, SEM standard error of mean. *p < .05 and ***$p < .001$.

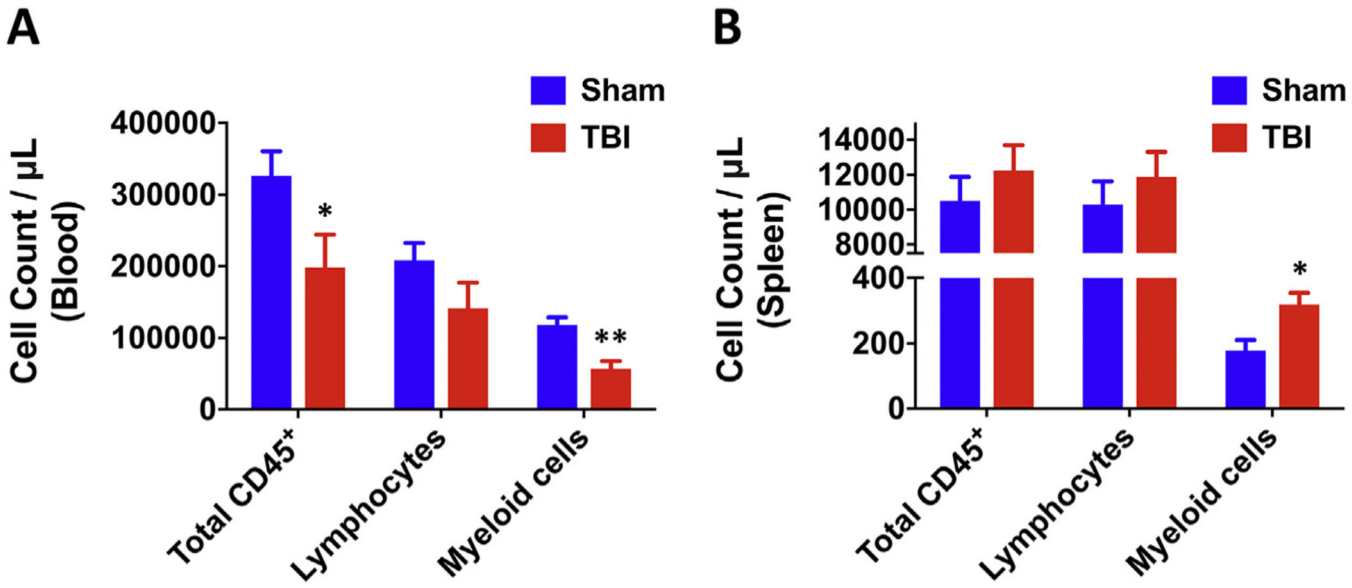


**Fig. 7.**

Chronic TBI causes long-term alterations in peripheral myeloid counts in the blood and spleen. Circulating blood leukocyte counts were estimated using counting beads ($N$ = 8–10/group). The data show a significant decrease in total $CD45^+$ and $CD45^+CD11b^+$ myeloid cells in the blood at 8 months post-injury (A). Splenic leukocyte counts were estimated using counting beads (N = 5/group). $CD45^+CD11b^+$ myeloid counts were significantly increased in the spleen of chronic TBI mice com- pared to sham controls (B). Statistical analysis was performed using two-way ANOVA with multiple comparisons. Error bars show mean SEM. Abbreviation: µL microliter, TBI traumatic brain injury, SEM standard error of mean. *p < .05 and **$p$ < .01.